

# PRISM: Lightweight Multivariate Time-Series Classification through Symmetric Multi-Resolution Convolutional Layers

Federico Zucchi<sup>a,b,\*</sup>, Thomas Lampert<sup>a</sup>

<sup>a</sup>*ICube, University of Strasbourg, Illkirch-Graffenstaden, France*

<sup>b</sup>*Cephalgo, Strasbourg, France*

---

## Abstract

Multivariate time-series classification is pivotal in domains ranging from wearable sensing to biomedical monitoring. Despite recent advances, Transformer- and CNN-based models often remain computationally heavy, offer limited frequency diversity, and require extensive parameter budgets. We propose PRISM (Per-channel Resolution-Informed Symmetric Module), a convolutional-based feature extractor that applies symmetric finite-impulse-response (FIR) filters at multiple temporal scales, independently per channel. This multi-resolution, per-channel design yields highly frequency-selective embeddings without any inter-channel convolutions, greatly reducing model size and complexity. Across human-activity, sleep-stage and biomedical benchmarks, PRISM, paired with lightweight classification heads, matches or outperforms leading CNN and Transformer baselines, while using roughly an order of magnitude fewer parameters and FLOPs. By uniting classical signal processing insights with modern deep learning, PRISM offers an accurate, resource-efficient solution for multivariate time-series classification.

---

## 1. Introduction

Multivariate time series data, characterised by intricate temporal dependencies, is prevalent across diverse fields such as finance, healthcare, environmental science, and human activity recognition. Recent advances in deep learning methodologies have considerably improved the analysis and classification capabilities for such data. Nevertheless, contemporary state-of-the-art models frequently encounter significant obstacles concerning computational efficiency, model complexity, and limited frequency diversity.

Transformer architectures, initially established in natural language processing owing to their capacity to model long-range dependencies, have recently been adapted to time series contexts. Despite demonstrating promising initial performance in capturing temporal correlations, Transformers are hindered by extensive parameterisation which may lead to overfitting issues [1]. While self-attention mechanisms are designed to be robust in theory, in practice they often underperform due to the significant noise and redundancy present in real-world time series [2, 3]. Moreover, recent empirical studies have underscored scenarios wherein simpler, single-layer linear models have surpassed the classification performance of sophisticated Transformer architectures, particularly on datasets characterised by limited scale and lower noise levels [4]. This discrepancy indicates a fundamental mismatch between Transformer complexity and many practical applications.

Conversely, convolutional neural networks (CNNs) have demonstrated considerable success in capturing short-term and

long-term temporal dynamics via multi-scale convolutional frameworks [5]. Even when paired with straightforward linear classifiers, they have been shown to achieve results comparable to more complex neural architectures, while maintaining a significantly reduced computational burden [6]. In addition, precise frequency selectivity and full-spectrum use are crucial for effective time-series representation [7]. Consequently, a pivotal research question emerges: How can one construct time-series models that simultaneously achieve high computational efficiency, spectral diversity in the representation, and predictive accuracy? In addressing this challenge, classical signal processing techniques, notably wavelet transforms, have historically provided transparent and well-characterised frequency-domain decompositions [8]. However, these traditional approaches are inherently limited in their adaptability [9]. In contrast, contemporary neural network architectures offer significantly greater flexibility and representational capacity. Hence, a secondary critical inquiry arises: Is it possible to integrate the frequency selectivity and spectral control of classical signal processing methods with the adaptive representational capabilities of modern deep learning frameworks?

Inspired by the fundamental principle of a prism splitting white light into distinct spectral components, we introduce PRISM (Per-channel Resolution-Informed Symmetric Module), a convolution-based feature extractor explicitly designed to separate multivariate time series data into frequency-rich embeddings that tend to be spectrally distinct. PRISM employs symmetric (palindromic) FIR convolutional filters, guaranteeing linear-phase behaviour that preserves the signal's phase and eliminates phase distortion [10]. This symmetry encourages diverse spectral responses, analogous to the separation of spectral components of light. Within PRISM, each channel is indepen-

---

\*Corresponding author

Email addresses: f.zucchi@unistra.fr (Federico Zucchi), lampert@unistra.fr (Thomas Lampert)

dently processed through symmetric convolutional filters spanning multiple scales.

The approach avoids complex inter-channel fusion or deep neural structures, thus maintaining simplicity and computational efficiency. Furthermore, symmetric filters inherently reduce parameter counts by approximately half per filter without sacrificing representational strength, significantly decreasing computational demands and limiting overfitting risks [11].

By combining classical multi-resolution analysis with modern neural adaptability, PRISM offers a pragmatic approach to multivariate time-series modelling. PRISM’s modular design aligns naturally with multiple and multi-modal sensor setups across diverse application domains. Empirical evaluations on a wide range of benchmark datasets demonstrate PRISM’s competitive or superior performance relative to traditional CNN and Transformer-based methods, alongside substantial reductions in complexity, computational resource consumption, and parameterisation. Additionally, the frequency selectivity induced by the symmetric FIR design provides spectral features that can facilitate analysis of the learned representations.

The contributions of this paper can be summarised as follows:

- **Parameter-efficient multi-scale convolution:** We introduce PRISM, a feature extractor using symmetric FIR filters at multiple temporal resolutions, which reduces parameter count while preserving representational power.
- **Frequency-diverse, less redundant filters:** We show that the symmetric design encourages frequency-selective features, minimises spectral redundancy, and yields diverse filters, as demonstrated by frequency analyses.
- **Versatile integration and strong empirical performance:** PRISM integrates seamlessly with different classification heads, achieving competitive or superior accuracy on diverse benchmarks with lower computational cost.
- **Extensive analysis and flexibility.** Systematic ablations and complexity studies verify the value of multi-resolution design and show that PRISM scales gracefully from low- to high-dimensional or multi-modal signals, remaining efficient under tight memory and FLOP budgets.

## 2. Related Works

### 2.1. Symmetric FIR Filters as CNN Feature Extractors

Recent advances have explored incorporating linear-phase constraints through symmetric (palindromic) finite impulse response (FIR) convolutional filters as initial layers in convolutional neural networks. Such symmetry enforces a linear-phase frequency response, thereby enabling predictable spectral behavior and facilitating analysis of the frequency characteristics of learned filters [11]. Specifically, symmetric FIR filters induce a response equivalent to a linear combination of cosine basis functions, analogous to discrete cosine transforms (DCT) [10, 12, 13], widely appreciated for their spectral compactness in signal compression tasks [14].

Ulicny et al. [14] explicitly leverage this concept by introducing Harmonic Convolutional Networks (HCN), wherein standard convolutional kernels are replaced by learnable weighted combinations of fixed DCT basis functions. This harmonic representation achieves comparable or superior performance to conventional CNNs while substantially reducing redundancy in the learned kernels. Such a structured representation demonstrates improved convergence speeds and enhanced generalisation, attributed directly to the reduced parameter complexity and the robustness of harmonic basis regularisation.

Moreover, SymNet [11] empirically demonstrates across various image classification benchmarks that imposing symmetry constraints on CNN kernels dramatically reduces parameter counts without significant loss of accuracy, suggesting an intrinsic redundancy in traditional convolutional parameterisation.

The integration of these filters serves as a regularisation technique, steering model learning toward frequency-selective, noise-robust feature extraction. Indeed, the empirical advantages reported in multiple studies, mainly in the image domain, include reduced computational load, accelerated training convergence, improved robustness to overfitting and spectral compactness [14, 15], provide strong theoretical and practical justifications for employing symmetric FIR filters as foundational CNN components.

As such, while prior work incorporates frequency-aware CNNs or filter constraints, no approach to date combines per-channel symmetric FIR filtering with multi-resolution design for multivariate time series.

### 2.2. Transformer-Based Networks

Since the seminal Transformer architecture was introduced for NLP [16], numerous studies have transplanted self-attention to time-series analysis. Early work such as Autoformer [17], FEDformer [18], LogSparse/Informer [19], Reformer [20], and Crossformer [21] highlighted the ability of attention to model long-range temporal interactions, achieving strong results in multivariate forecasting.

However, recent evidence questions the universal superiority of Transformers for time series. Zeng et al. [22] demonstrate that the permutation-invariant self-attention mechanism can dilute chronological order, sometimes allowing a one-layer linear model to outperform deep Transformers. Follow-up work shows that lightweight MLP architectures (e.g. DLinear [23]) rival Transformer forecasters with far fewer parameters. Moreover, Transformers typically demand large datasets and considerable compute; Wen et al. [1] report consistent overfitting on small or noisy benchmarks unless extensive regularisation is used. Quadratic memory in sequence length and high sensitivity to high-frequency noise further hinder their practicality [24]. These limitations motivate alternatives that embed stronger temporal inductive biases while remaining computationally efficient.

### 2.3. Convolution-Based Networks

One-dimensional CNNs excel at learning local motifs in time series and form the backbone of many state-of-the-art classi-

fication models. ROCKET uses thousands of random convolutional kernels to achieve competitive accuracy with minimal training cost [25]. Self-supervised frameworks such as TS-TCC [26], TS2Vec [27], and MHCCL [28] rely on CNN encoders to learn transferable representations.

To overcome CNNs’ limited receptive field, recent work incorporates multiresolution or frequency-aware designs. T-WaveNet introduces wavelet-based decomposition to separate low and high-frequency components [29]. SCINet recursively *down-sample–convolve–interact* subsequences, capturing long-term dependencies without attention [30]. WFTNet fuses Fourier and wavelet transforms inside a CNN to cover the full temporal spectrum [31]. TCE regularises 1D-CNNs to focus on informative low-frequency bands [32], while BTSF learns bilinear temporal–spectral features for unsupervised representation learning [33]. TimesNet reforms forecasting as multi-period analysis in a 2-D space, letting convolutional blocks learn both intra- and inter-period patterns [6].

Beyond the specific methods that adopt symmetric filters, as discussed in Section 2.1, recent work has increasingly focused on making the filters themselves adaptive and frequency-aware. FilterNet employs convolutional kernels that are explicitly trained to act as frequency-selective band-pass filters, enabling the model to match Transformer-level accuracy with far fewer parameters [7].

These advances show that modern CNNs, augmented with multi-scale processing, spectral priors, and structurally constrained filters, can rival or exceed Transformers in accuracy while remaining more robust on small datasets and dramatically more efficient in FLOPs and memory.

Our work continues the trajectory of convolutional approaches by incorporating symmetric kernels for phase-preserving, frequency diverse feature extraction.

### 3. Methodology

#### 3.1. Overview

The proposed feature extraction pipeline integrates two core modules: a symmetric multi-resolution feature extraction stage and a resolution-informed patch embedding. As shown in Figure 1, for each input channel, the signal is processed in parallel by several learnable, symmetric convolutional filters with different kernel sizes; for each resolution (kernel size), multiple filters are learned. The outputs from all filters are concatenated and passed to a patch-embedding module, which first applies a depth-wise convolution to create resolution-specific patch features, and then a point-wise (1×1) projection that fuses them into a single feature vector.

Figure 2 illustrates the extension to the multichannel setting, where each channel is processed independently using the same sequence of modules. The resulting embeddings from all channels are then stacked to form the output of the PRISM feature–extraction pipeline. Depending on the downstream application, the output can be aggregated by mean-pooling or kept at full temporal resolution.

#### 3.2. Multi Resolution Symmetric Module

Given an input channel  $x^{(i)} \in \mathbb{R}^T$ , we employ several convolutional filters of varying odd lengths  $\{k_1, \dots, k_{n_k}\}$ , with multiple filters for each size. Every filter  $w^{(f,k)} \in \mathbb{R}^k$  satisfies the symmetry property  $w_{-j}^{(f,k)} = w_j^{(f,k)}$ , meaning its weights are mirrored around the center.

This symmetry ensures that each filter produces outputs without phase distortion, preserving the alignment of the original input data. Specifically, the convolution operation centers the symmetric filter at each time step and sums the products of input values with the corresponding filter weights, ensuring accurate temporal alignment:

$$h_{t,f}^{(i,k)} = \sum_{j=-\lfloor k/2 \rfloor}^{\lfloor k/2 \rfloor} w_j^{(f,k)} x_{t+j}^{(i)}.$$

By using filters of multiple sizes, we extract features sensitive to different time scales:

- Smaller filters capture short-term patterns with higher temporal detail.
- Larger filters capture broader trends with lower frequency selectivity.

Then, the  $\ell_2$ -normalisation:

$$w^{\text{norm}} = \frac{w}{\|w\|_2 + \epsilon}, \quad (1)$$

enforces unit filter energy  $\langle w^{\text{norm}}, w^{\text{norm}} \rangle = 1 + O(\epsilon)$ , preventing gradient updates from altering filter gain disproportionately to shape. This preserves the designed frequency response characteristics during training while maintaining numerical stability.

The architecture forms a multi-resolution bank of learnable symmetric FIR filters: for each kernel size we learn  $n_f$  parallel symmetric kernels.

#### 3.3. Resolution–Informed Patch Embedding

The feature matrix  $h^{(i)} \in \mathbb{R}^{T \times F}$  is segmented into overlapping temporal patches of length  $p$  and stride  $p/2$ , yielding  $L_p$  patches per channel. This patching ensures both local context and temporal continuity are preserved.

Each patch is first processed by a *depth-wise* convolution:

$$z_{\ell,f}^{(i)} = \sum_{j=0}^{p-1} v_j^{(f)} h_{\ell p/2+j,f}^{(i)} \quad \ell = 1, \dots, L_p \quad (2)$$

where  $v^{(f)} \in \mathbb{R}^p$  is a learnable filter specific to each resolution channel  $f$ . This operation preserves the independence of resolution bands, allowing the model to extract resolution–informed temporal features within each patch.

Subsequently, features are *fused across resolutions* using a point-wise linear projection:

$$X_\ell^{(i)} = \sum_{f=1}^F \mathbf{p}_f z_{\ell,f}^{(i)}, \quad \mathbf{p}_f \in \mathbb{R}^D. \quad (3)$$

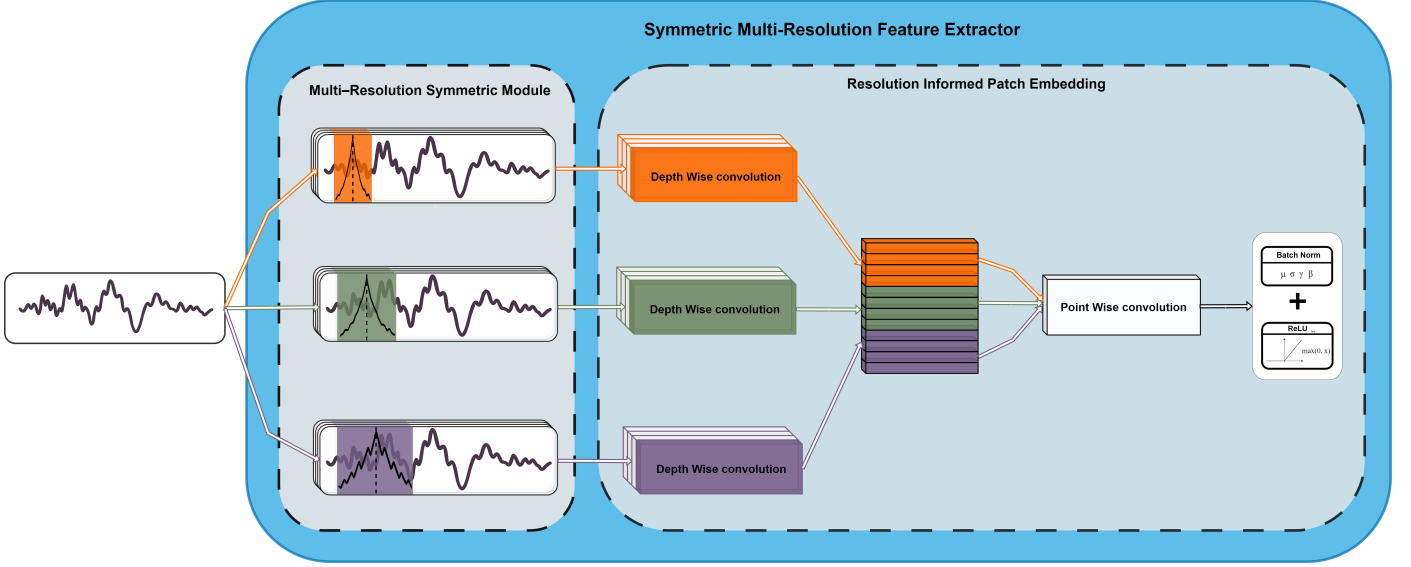


Figure 1: Overview of the proposed architecture. The symmetric multi-resolution feature-extraction module (shown here for a single input channel) works as follows. For each resolution, a set of learnable symmetric convolutional filters (four per resolution in this example) with distinct odd kernel sizes is applied in parallel to the input signal. The filtered outputs are concatenated and fed to the patch-embedding block, where a depth-wise convolution first tokenises each resolution band, and a subsequent point-wise ( $1 \times 1$ ) projection fuses them into a unified feature vector. The resulting tokens pass through BatchNorm, a ReLU activation, and dropout.

Here each  $\mathbf{p}_f$  is a learnable  $D$ -dimensional vector that projects the  $f$ -th resolution channel into the shared embedding space; their sum aggregates local temporal and cross-resolution information.

The resulting sequence  $X^{(i)} \in \mathbb{R}^{L_p \times D}$  forms a set of patch tokens, each representing a localised, resolution-aware embedding. This design translates rich time-frequency patterns into a compact representation suitable for downstream sequence models, while maintaining the original temporal order. Overlapping patches further enhance feature continuity and robustness to local variations.

### 3.4. Channel-Wise Pooling and Normalisation

Each patch token is first normalised by an *affine LayerNorm*,  $\mathcal{N}_i$ :

$$\hat{X}_\ell^{(i)} = \mathcal{N}_i(X_\ell^{(i)}), \quad \ell = 1, \dots, L_p.$$

LayerNorm standardises every token to zero mean and unit variance across its  $D$  embedding dimensions.

We then obtain a compact representation by *temporal pooling*, averaging the normalised tokens along the patch axis:

$$r^{(i)} = \frac{1}{L_p} \sum_{\ell=1}^{L_p} \hat{X}_\ell^{(i)} \in \mathbb{R}^D. \quad (4)$$

This aggregation summarises the temporal dynamics of modality  $i$  in a single  $D$ -dimensional vector.

### 3.5. Output Interface

Figure 2 provides a visual summary of how the modality-specific patch embeddings are aggregated into the final output representation, both *without* and *with* the optional mean-pooling stage.

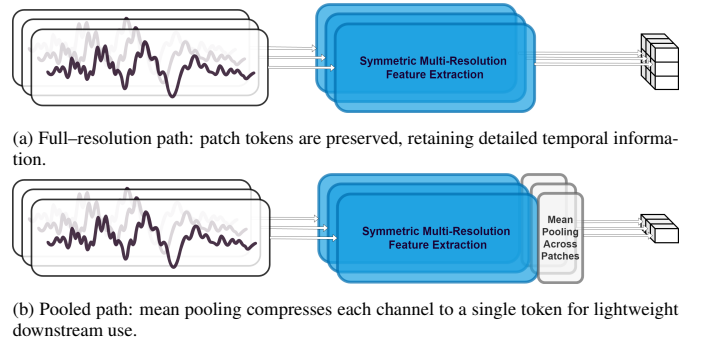


Figure 2: PRISM output interface. (a) supports fine-grained temporal analysis, while (b) offers a compact summary when only global channel information is required (see Eq. (4)).

The pooled front-end output is the concatenation of the  $C$  modality vectors

$$R = [r^{(1)}, \dots, r^{(C)}] \in \mathbb{R}^{B \times C \times D},$$

where  $B$  denotes the batch size (cf. Fig. b).

If the pooling step in Eq. (4) is skipped, the model outputs one token matrix  $X^{(i)} \in \mathbb{R}^{B \times L_p \times D}$  per channel, preserving full temporal resolution for downstream sequence-level modelling (cf. Fig. a).

### 3.6. Model Complexity Analysis

We characterise the computational and memory complexity of PRISM by decomposing its operations into distinct stages. Let  $B$  denote the batch size,  $C$  the number of input channels,  $T$  the sequence length,  $n_k$  the number of odd kernel sizes  $\{k_1, \dots, k_{n_k}\}$ , and  $n_f$  the number of symmetric filters per size. The total number of filters is  $F = n_k n_f$ , with average kernel

length  $\bar{k} = \frac{1}{n_k} \sum_{m=1}^{n_k} k_m$ . For the patch embedding, the number of overlapping patches is  $L_p \approx \frac{2T}{p}$ , where  $p$  is the patch size (stride  $p/2$ ), and  $D$  is the embedding dimension.

**Filter-Bank Stage.** Each input channel is convolved with  $F$  depth-wise symmetric filters of length  $\bar{k}$ , producing

$$O(BCFT\bar{k})$$

multiply-accumulate operations and requiring

$$O(CF\bar{k})$$

parameters.

**Patch Embedding Stage.** Each filtered channel is partitioned into  $L_p$  patches. For each patch, a depth-wise convolution (length  $p$ ) is followed by a pointwise ( $1 \times 1$ ) projection to  $D$  dimensions. The computational complexity is

$$O(BCFL_p(p+D)),$$

with parameter count per channel

$$O(Fp + FD + D) = O(F(p+D) + D).$$

**Pooling, Normalisation, Output.** The pooling operation (mean over  $L_p$  patches) incurs

$$O(BCDL_p)$$

operations. LayerNorm contributes

$$O(CD)$$

additional parameters. The output dimensionality is  $(B, C, D)$  for pooled or  $(B, C, L_p, D)$  for unpooled representations.

All principal hyperparameters  $(C, F, \bar{k}, T, p, D)$  influence computational and parameter complexity in a linear fashion. The scaling of  $p$  and  $L_p$  is inversely proportional, while  $F$  and  $\bar{k}$  directly affect frequency resolution and cost. The architecture thus allows for precise, linear resource allocation and predictable trade-offs between computational efficiency and representational capacity.

## 4. Experiments on Benchmark Datasets

### 4.1. Datasets

To evaluate our model, we adopted publicly available datasets from two representative domains: biomedical signals and human activity recognition (HAR). These datasets are widely used benchmarks in the time series community and cover a broad range of classification tasks, enabling a comprehensive assessment of our model’s performance.

More precisely, data was made available through public repositories, this guarantees full reproducibility of our experiments and direct comparability with existing methods. The datasets span a diverse range of channel counts, signal lengths, and training sample sizes, providing a comprehensive testbed for evaluating model capabilities. These characteristics are summarised in Table 1.

In the following, we report the datasets used and summarise the preprocessing applied to the data.

Table 1: Dataset statistics: number of training and testing samples, sequence length, number of channels, and classes.

| Dataset   | # Train | # Test | Length | # Channels | # Classes |
|-----------|---------|--------|--------|------------|-----------|
| UCIHAR    | 7,352   | 2,947  | 128    | 9          | 6         |
| WISDM     | 4,731   | 2,561  | 128    | 3          | 6         |
| HHAR      | 10,336  | 4,436  | 128    | 3          | 6         |
| Sleep EEG | 25,612  | 8,910  | 3,000  | 1          | 5         |
| ECG       | 87554   | 21892  | 187    | 1          | 2         |
| Heartbeat | 163     | 204    | 205    | 61         | 2         |

**Sleep-EDF Dataset** The Sleep-EDF dataset, sourced from PhysioBank [34], comprises whole-night polysomnography (PSG) recordings used primarily for sleep stage classification. Specifically, only EEG signals from the Fpz-Cz channel were extracted, all with a sampling rate of 100 Hz, consistent with previous studies [35, 26, 36]. The task involved classifying EEG signals into one of five sleep stages: Wake (W), Non-Rapid Eye Movement (N1, N2, N3), and Rapid Eye Movement (REM).

**MIT-BIH Arrhythmia Dataset (ECG)** The MIT-BIH Arrhythmia Dataset [37], hosted on PhysioNet, comprises electrocardiogram (ECG) recordings curated for the purpose of arrhythmia detection and classification. Recognised as a benchmark dataset in cardiovascular research, it offers a rigorously annotated collection of heartbeats and arrhythmic events, and is extensively employed for the development and validation of arrhythmia detection methodologies.

**Heartbeat Dataset** Heartbeat [38] dataset comprises five-second sound recordings of heartbeats collected for the PhysioNet/CinC Challenge 2016 in both clinical and nonclinical environments at sites such as the aortic, pulmonic, tricuspid and mitral areas. Recordings are labeled as normal (from healthy subjects) or abnormal (from patients with diagnosed cardiac conditions such as valve defects and coronary artery disease).

**UCI HAR Dataset** The UCI HAR dataset [39] includes sensor readings from 30 subjects performing six activities (walking, walking upstairs, downstairs, standing, sitting, and lying down). Data was collected using a Samsung Galaxy S2 smartphone mounted at the waist, capturing accelerometer and gyroscope data sampled at 50 Hz.

**WISDM Dataset** The WISDM dataset [40] provides time series data collected from smartphones and wearable devices during activities such as walking, jogging, sitting, and standing. It enables the evaluation of robustness across a variety of motion patterns and sensor placements.

**HHAR Dataset** The HHAR dataset [41] stands out due to its heterogeneity, provides data from multiple device types (smartphones and smartwatches) across various activities such as biking, sitting, standing, walking, and stair climbing. This variability provides a challenging benchmark for evaluating a model’s generalisation capabilities across different sensor configurations.

## 4.2. Training Protocol and Objective Function.

For all classification experiments, we closely followed the training protocol established in the TSLANet [36] paper to ensure comparability. Models were optimised using the AdamW optimiser, with a learning rate of  $1 \times 10^{-3}$  and a weight decay of  $1 \times 10^{-4}$ . Each experiment was run for 100 epochs, with model selection based on the checkpoint achieving the lowest validation loss.

We employed the categorical cross-entropy loss function with label smoothing. This loss is defined as:

$$\mathcal{L}_{\text{clf}} = - \sum_{i=1}^C y_i^{\text{smooth}} \cdot \log(\hat{y}_i), \quad (5)$$

where  $y_i^{\text{smooth}} = (1 - \epsilon) \cdot y_i + \epsilon/C$ , with  $\epsilon$  as the smoothing parameter,  $y_i$  the true class label in one-hot encoding,  $\hat{y}_i$  the predicted probability for class  $i$ , and  $C$  the number of classes. Label smoothing helps to mitigate overconfidence in model predictions and improves generalisation.

All experiments were run with the same set of hyperparameters: convolutional kernel sizes of 11, 21, 51 and 71 and an embedding size of 128 for the final convolutional layer. Intermediate depthwise convolutional layers employed a kernel size of 8. Model performance was evaluated using classification accuracy, in line with established benchmarks for the selected datasets [36, 26].

## 4.3. Model Variants

To systematically assess the flexibility and effectiveness of PRISM as a generic feature learning front-end, we explored its integration with various classification heads, each representing different levels of model complexity and representational power. Specifically, we evaluated three distinct head architectures:

- **Linear Head** As a baseline, we attached a single linear (fully connected) layer directly on top of the output of PRISM’s patch embedding module. This head projects the learned features into the class space, providing a straightforward mapping from the latent feature space to the target labels. This setup allows us to isolate the feature extraction capability of PRISM by minimising the modeling capacity of the classification head.
- **Multi-Layer Perceptron (MLP) Head** To test whether a more expressive, non-linear mapping can leverage the representations learned by PRISM, we employed a simple MLP consisting of one hidden layer with ReLU activation. This architecture increases the modeling flexibility of the head while remaining relatively lightweight, thus enabling us to investigate whether additional non-linearity is beneficial for classification performance.
- **Transformer-Based Head** To explore the potential of modeling inter-feature dependencies and sequence-level interactions, we further experimented with a transformer encoder as the classification head. Here, we prepended a learnable [CLS] token to the PRISM feature sequence, allowing the

transformer to aggregate sequence-wide information for classification. We considered two variants for integrating the transformer head:

- *Pooled.* The output features from PRISM were first averaged along the channel dimension, resulting in a single feature vector per input sample. This pooled representation was then fed into the transformer encoder.
- *Unpooled.* Instead of pooling, the full set of PRISM features (i.e., one vector per channel) was stacked and provided directly to the transformer, allowing it to operate on the complete set of channel-wise embeddings.

This systematic exploration provides insights into the complementarity between PRISM’s feature learning and various classification strategies, from simple linear mappings to more complex architectures capable of modeling higher-order relationships.

## 4.4. Baselines

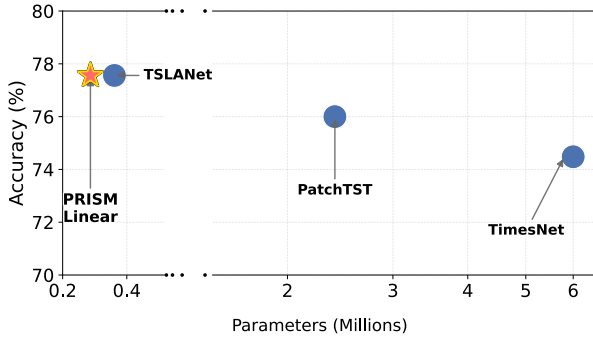
To assess classification performance, PRISM and its variants are evaluated against a range of state-of-the-art methods, including TSLANet [36], GPT4TS [42], TimesNet [6], ROCKET [25], TS-TCC [26], TS2Vec [27], Crossformer [21], and PatchTST [43]. These represent leading Transformer-based and convolutional architectures in recent literature. All baseline results are sourced from the TSLANet paper [36] to ensure consistency and fair comparison.

## 4.5. Results

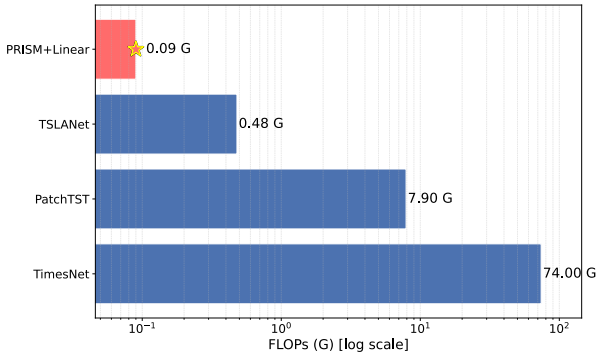
Table 2 reports comparative results between our proposed feature extractor in combination with different downstream classifiers and the baselines. The PRISM architecture, evaluated with various classifier heads, demonstrates robust and highly competitive performance across all tested datasets.

When comparing PRISM variants to leading transformer-based methods, such as GPT4TS and CrossFormer, as well as with advanced convolutional architectures like ROCKET and TSLANet, PRISM consistently matches or outperforms them. Particularly noteworthy is that the PRISM-Linear variant, which only uses a simple linear classification layer atop the learned embeddings, already achieves accuracy on par with the most complex transformer-based solutions. This result strongly suggests that the quality of representations learned by PRISM’s structured convolutional front-end is sufficient to capture the relevant temporal and frequency dynamics required for state-of-the-art performance, even with minimal classifier complexity. It is important to note that this performance is achieved with a model size that is orders of magnitude smaller: for example, TSLANet requires about 500k parameters for 3-channel HHAR\_SA and up to 9-channel UCIHAR, whereas PRISM combined with a linear layer uses only about 13k parameters (HHAR\_SA) or 40k (UCIHAR).

In addition, we compared against the recent self-supervised representation learning methods TS-TCC and TS2Vec, both of which rely on a contrastive learning based pre-training phase before linear evaluation. Despite not using any separate pre-training PRISM consistently surpasses TS2Vec and remains



(a) PRISM+Linear vs. baselines: number of parameters vs. accuracy (UEA Heartbeat).



(b) PRISM+Linear vs. baselines: FLOPs vs. accuracy (UEA Heartbeat).

Figure 3: Comparison of PRISM+Linear and baselines in terms of (a) parameter count and (b) FLOPs versus classification accuracy on the UEA Heartbeat dataset.

within a narrow margin of TS-TCC across the board. This further underlines the strength of the features extracted by PRISM without the overhead of extra training stages.

Using a more complex classification head, such as a Transformer with self-attention, provides only a slight improvement in accuracy compared to the linear or MLP heads. This observation is consistent with recent literature, which has shown diminishing returns from increasing classifier complexity when high-quality embeddings are provided by the feature extractor [36, 23]. The capacity of the PRISM-Transformer variants to effectively leverage self-attention without substantial redesign further attests to the generality and discriminative power of the underlying embeddings.

In summary, the results from Table 2 clearly demonstrate that PRISM delivers state-of-the-art performance across diverse time series tasks, with notable efficiency. The model’s effectiveness with a simple linear head highlights the central importance of robust, structured feature extraction. At the same time, its compatibility with Transformer heads showcases the versatility and strength of PRISM’s learned representations, which may be readily adopted in more complex downstream pipelines where further accuracy is needed.

#### 4.6. Complexity Analysis

To assess both model complexity and computational footprint, we evaluate these aspects for PRISM as well as for the best-performing (without pre-training) transformer-based

(PatchTST) and CNN-based baselines (TSLANet, TimesNet) reported in Table 2. This comparison allows a fair assessment of efficiency alongside predictive performance.

Following Eldele et al. [36], we evaluate PRISM on the UEA Heartbeat dataset, a benchmark chosen specifically for its high channel count (61 dimensions) and limited sample size (a few hundred recordings), in order to stress-test scalability and over-fitting risk. As shown in Figure 3a, PRISM’s per-channel design grows linearly to only  $\sim 2.7 \times 10^5$  parameters, still well below TSLANet’s  $\sim 4.0 \times 10^5$  and an order of magnitude smaller than PatchTST counterparts ( $\sim 2.3M$ ). Regarding compute cost (Figure 3b), the compute footprint remains at just  $\sim 0.09$  GFLOPs, yielding a  $5.3\times$  reduction versus TSLANet and a 99% reduction versus PatchTST. Despite this minimal footprint, PRISM achieves 77.56% accuracy, equaling TSLANet, and superior to PatchTST (75.6%) and TimesNet (74.48%).

In summary, even under high-dimensional, low-sample conditions, PRISM scales gracefully with channel count yet remains lighter than published state of the art, while matching or exceeding their accuracy. This confirms that carefully designed, domain-specific architectural choices such as per-channel symmetric filtering and multi-resolution decomposition can match or surpass the efficiency and performance of much larger generic models in time-series classification.

## 5. Case Study: ISRUC-S3 Dataset

### 5.1. Motivation and Context

While PRISM demonstrates strong performance on widely used public benchmarks, we further evaluate its capabilities on the ISRUC-S3 dataset a multimodal sleep stage classification task that presents significant additional challenges. ISRUC-S3 is not only more complex due to the diversity of sensor modalities involved (EEG, EOG, EMG, ECG), but it also reflects practical constraints commonly encountered in clinical scenarios, such as limited subject numbers.

By testing PRISM under these demanding conditions, we stress the architecture’s robustness and highlight its suitability for real-world applications. In particular, this experiment underscores two key strengths of PRISM: (1) its ability to efficiently integrate and process information from multiple, sensor-specific channels, and (2) its exceptionally small computational footprint both in terms of MFLOPs and parameter count which is critical for deployment in resource-constrained environments, such as wearable devices or bedside monitoring systems. This evaluation therefore goes beyond standard benchmarks to demonstrate that PRISM is not only effective, but also practical and scalable for challenging, real-world use cases.

### 5.2. Dataset Description

The ISRUC-S3 dataset [44] consists of polysomnographic recordings from 10 healthy subjects collected during sleep. The signals are segmented into 30-second epochs, yielding a total of 8,589 samples. Sleep stages are annotated by two experts according to the AASM standard, resulting in five classes:

Table 2: Classification accuracy (%) of all methods on human-activity (left) and biomedical (centre) datasets, plus per-block and overall averages (right). Best in **blue bold**, second in **red underlined**.

| Model                | Human Activity |              |              | Avg (HAR)    | Biomedical   |              |              | Avg (Bio)    | Total Avg    |
|----------------------|----------------|--------------|--------------|--------------|--------------|--------------|--------------|--------------|--------------|
|                      | UCIHAR         | WISDM        | HHAR.SA      |              | EEG          | ECG          | Heartbeat    |              |              |
| TSLANet              | 96.06          | 97.77        | <b>98.53</b> | <b>97.46</b> | 82.10        | 98.37        | <b>77.56</b> | 86.01        | 91.73        |
| GPT4TS               | 91.24          | 89.49        | 97.40        | 92.71        | 76.37        | 97.70        | 36.59        | 70.22        | 81.46        |
| TimesNet             | 91.34          | 89.61        | 93.59        | 91.51        | 75.86        | 98.33        | 74.48        | 82.89        | 87.20        |
| ROCKET               | 94.37          | 97.03        | 97.93        | 96.44        | 76.69        | 97.72        | 69.76        | 81.39        | 88.92        |
| CrossFormer          | 76.59          | 77.31        | 78.74        | 77.55        | 53.30        | 88.33        | 76.59        | 72.74        | 75.14        |
| PatchTST             | 92.70          | 95.94        | 95.96        | 94.87        | 69.69        | 98.06        | 76.59        | 81.45        | 88.16        |
| TS-TCC               | 95.95          | 97.05        | 98.49        | 97.16        | <b>86.06</b> | <b>98.44</b> | <b>77.07</b> | <b>87.19</b> | <b>92.18</b> |
| TS2VEC               | 96.19          | 93.87        | 97.05        | 95.70        | 75.13        | 97.48        | 69.76        | 80.79        | 88.25        |
| PRISM-Linear         | <b>97.32</b>   | 96.21        | 98.30        | 97.28        | <b>84.18</b> | 95.72        | <b>77.56</b> | 85.82        | 91.55        |
| PRISM-MLP            | 96.47          | 97.54        | 98.20        | 97.40        | 83.39        | 98.37        | 71.70        | 84.49        | 90.94        |
| PRISM-Transf. pool   | 95.62          | <b>97.94</b> | 98.08        | 97.21        | 83.50        | 98.11        | <b>77.56</b> | <b>86.39</b> | <b>91.80</b> |
| PRISM-Transf. unpool | <b>96.74</b>   | <b>97.81</b> | <b>98.51</b> | <b>97.69</b> | 82.88        | <b>98.81</b> | 75.12        | 85.60        | 91.64        |

Wake, N1, N2, N3, and REM. The dataset includes six referenced EEG channels, two EOG channels, one EMG channel, and one ECG channel, all downsampled to 100 Hz. Consistent with previous work [45], the ECG channel is excluded from analysis due to its periodic nature. To suppress high-frequency noise, each channel is preprocessed using a fourth-order low-pass Butterworth filter with a 40 Hz cutoff.

### 5.3. Experimental Protocol

The evaluation on ISRUC-S3 follows a 10-fold repeated subject-wise cross-validation, as recommended in prior work. Given the small number of subjects, cross-validation is repeated 10 times with fixed folds across repetitions to ensure robust estimates despite potential overlap between test subjects across folds. This protocol addresses the reduced effective sample size and provides a fair basis for model comparison.

To ensure consistency and facilitate a direct comparison, all experiments and performance assessments are conducted within the same framework and evaluation pipeline as the original MSA-CNN study [45]. Reported results for comparative methods are taken directly from the evaluation presented in that work.

Analogous to the “small” configuration explored for MSA-CNN study, we also evaluated a lightweight variant of PRISM on the ISRUC-S3 dataset: convolutional kernel sizes of 7, 15, and 25 in the temporal-convolution blocks, an embedding dimension of 26 in the final convolutional layer, and depth-wise convolutional layers with a kernel size of 8 at intermediate stages.

All experiments in this section use the PRISM front-end followed by a single linear classification layer.

### 5.4. Evaluation Metrics

Model performance is reported using three complementary metrics:

- **Accuracy:** The proportion of correctly classified samples across all sleep stages.
- **Macro F1 Score:** The unweighted mean of F1-scores computed per class, which mitigates class imbalance effects.

- **Cohen’s Kappa:** Measures the agreement between predicted and true labels while correcting for chance, providing a robust assessment in the presence of class imbalance.

For each metric, results are first averaged over test folds (weighted by the number of samples per fold), then averaged across all repetitions.

### 5.5. Baselines

PRISM is tested against state-of-the-art methods specifically developed for sleep stage classification using raw EEG signals, without relying on hand-crafted features. These include convolutional and recurrent models such as DeepSleepNet [46], which combines CNNs for feature extraction with bidirectional LSTMs for modeling temporal transitions, and EEGNet [47], which uses depthwise-separable convolutions for efficient temporal and spatial filtering. Other approaches, like AttnSleep [35], integrate multi-resolution CNNs with attention mechanisms to capture both frequency-specific patterns and long-range dependencies. A distinct class of models—including MSTGCN [48], JK-STGCN [49], HierCorrPool [50], and FC-STGNN [51], leverages graph neural networks to encode spatial and temporal relationships across EEG channels or multimodal inputs. Finally, models like cVAN [52] and MSA-CNN [45] combine CNN-based spectral encoders with Transformer-like attention blocks to align and contextualise temporal representations at multiple scales.

### 5.6. Results and Discussion

PRISM demonstrates a compelling balance between classification performance and computational efficiency. Although MSA-CNN achieves higher absolute scores, PRISM yields closely comparable results across all metrics, with an average gap of less than 2 percentage points. Notably, PRISM consistently outperforms or matches the performance of several larger and more complex architectures, as reported in Table 3.

Crucially, PRISM achieves this level of performance while maintaining the lowest computational and architectural footprint among all models evaluated. As detailed in Table 4, PRISM requires only 3,817 parameters and 8.3 MFLOPS. In

Table 3: Classification results on the ISRUC-S3 dataset (multivariate) in terms of mean  $\pm$  std (%).

| Method                    | Accuracy                         | Macro F1                         | Kappa                            |
|---------------------------|----------------------------------|----------------------------------|----------------------------------|
| EEGNet                    | 75.9 $\pm$ 1.0                   | 71.9 $\pm$ 1.0                   | 68.2 $\pm$ 1.3                   |
| GraphSleepNet             | 69.8 $\pm$ 1.7                   | 66.7 $\pm$ 2.1                   | 60.3 $\pm$ 2.1                   |
| MSTGCN                    | 77.2 $\pm$ 0.6                   | 73.5 $\pm$ 0.7                   | 69.7 $\pm$ 0.7                   |
| JK-STGCN                  | 75.9 $\pm$ 0.6                   | 72.0 $\pm$ 0.4                   | 68.1 $\pm$ 0.7                   |
| HierCorrPool              | 72.1 $\pm$ 1.3                   | 67.8 $\pm$ 1.6                   | 63.1 $\pm$ 1.7                   |
| FC-STGNN                  | 68.6 $\pm$ 0.4                   | 64.6 $\pm$ 1.0                   | 58.5 $\pm$ 0.8                   |
| cVAN                      | 72.5 $\pm$ 2.0                   | 67.7 $\pm$ 2.5                   | 63.7 $\pm$ 2.5                   |
| MSA-CNN (small)           | 79.8 $\pm$ 0.9                   | 76.8 $\pm$ 1.1                   | 73.2 $\pm$ 1.1                   |
| PRISM Linear Small (ours) | <b>78.1 <math>\pm</math> 0.5</b> | <b>74.8 <math>\pm</math> 0.6</b> | <b>71.1 <math>\pm</math> 0.6</b> |

Table 4: Parameters and FLOPs of PRISM+Linear on the ISRUC-S3 dataset

| Model                     | # parameters | MFLOPS     |
|---------------------------|--------------|------------|
| EEGNet                    | 12,181       | 32.8       |
| MSTGCN                    | 476,292      | 204.0      |
| JK-STGCN                  | 458,085      | 208.6      |
| HierCorrPool              | 13,290,000   | 499.0      |
| FC-STGNN                  | 3,200,000    | 475.8      |
| cVAN                      | 6,834,571    | 483.4      |
| MSA-CNN (small)           | 10,583       | 19.8       |
| <b>PRISM+Linear(ours)</b> | <b>3,817</b> | <b>8.3</b> |

comparison, MSA-CNN, the next most lightweight model, uses nearly three times as many parameters and over twice the number of MFLOPS. Graph-based architectures such as HierCorrPool and FC-STGNN are even more demanding, exceeding PRISM’s parameter count by factors of over  $10^3$  and requiring more than 95% additional floating-point operations.

This reduction in resource demands does not come at a cost to predictive performance. For example, PRISM exceeds HierCorrPool by over 6 percentage points in accuracy and more than 7 in macro F1-score, despite having less than 0.03% of its parameters and approximately 1.6% of its MFLOPS. Compared to cVAN and FC-STGNN, PRISM maintains superior classification performance while remaining significantly more efficient in both model size and computational cost.

## 6. Model Analysis

### 6.1. Ablation Study and Discussion

To better understand the contributions of our multi-scale design, we performed ablation experiments analysing (1) the effect of increasing the number of temporal scales (resolution), and (2) the impact of varying the number of kernels per scale. Results for two representative datasets, WISDM and HHAR-SA, are reported below.

**Resolution ablation (number of scales)** We begin by varying the number of temporal scales, always starting from a single kernel length (15), and then incrementally adding kernels of length 31, 51, and 71. At each step, all previous scales are retained, so the kernel set grows cumulatively. Table 5 summarises the observed accuracy.

The results show that introducing additional temporal scales leads to consistent improvements in accuracy across both datasets. The largest jump is generally observed when moving from one to two scales, but further gains are achieved by

Table 5: Resolution Ablation ( $n_k=1$ ): Accuracy as a function of the number of temporal scales, with one kernel per scale.

| Dataset | # Scales | Kernel set  | Accuracy (%) | $\Delta$ vs. 1-scale |
|---------|----------|-------------|--------------|----------------------|
| WISDM   | 1        | 15          | 87.43        | –                    |
| WISDM   | 2        | 15–31       | 91.60        | +4.17                |
| WISDM   | 3        | 15–31–51    | 92.58        | +5.15                |
| WISDM   | 4        | 15–31–51–71 | 94.88        | +7.45                |
| HHAR-SA | 1        | 15          | 88.95        | –                    |
| HHAR-SA | 2        | 15–31       | 94.72        | +5.77                |
| HHAR-SA | 3        | 15–31–71    | 96.53        | +7.58                |
| HHAR-SA | 4        | 15–31–51–71 | 97.23        | +8.28                |

Table 6: Kernel-Count Ablation: Accuracy as a function of the number of kernels per scale, with a fixed set of temporal resolutions.

| Dataset | Kernels/scale | Accuracy (%) | $\Delta$ vs. 1 kernel |
|---------|---------------|--------------|-----------------------|
| WISDM   | 1             | 92.58        | –                     |
| WISDM   | 2             | 95.98        | +3.40                 |
| WISDM   | 3             | 96.92        | +4.34                 |
| WISDM   | 4             | 96.99        | +4.41                 |
| HHAR-SA | 1             | 97.23        | –                     |
| HHAR-SA | 2             | 97.75        | +0.52                 |
| HHAR-SA | 3             | 98.20        | +0.97                 |
| HHAR-SA | 4             | 98.26        | +1.03                 |

extending to three and four scales. This confirms that combining information from multiple temporal windows provides substantial benefits over single-scale approaches.

**Kernel-count ablation (kernels per scale)** To assess the effect of capacity at each scale, we next vary the number of kernels per resolution while holding the scale set fixed.

Increasing the number of kernels per scale also leads to accuracy gains, with each additional kernel offering some improvement. However, compared to the effect of adding new temporal scales, the magnitude of these gains is generally more moderate, especially in HHAR-SA, where the most significant improvements come from structural diversity in scale rather than kernel count.

Taken together, these results indicate that both multi-scale structure and increased filter capacity contribute to improved classification accuracy. Adding new temporal resolutions consistently drives substantial performance increases, while additional kernels per scale can further boost accuracy, but not as drastically. In practice, we find that covering a range of temporal windows is especially beneficial, and that supplementing each scale with multiple kernels can further refine performance when needed.

### 6.2. Effect of Symmetric Filtering on Filter Diversity

To rigorously assess the effect of symmetry constraints on convolutional filter learning, we conducted an empirical analysis comparing models with symmetric and asymmetric filter banks. Both models were trained under identical architectures, optimisation procedures, filter normalisation, and training protocols, ensuring that any observed differences could be attributed solely to the symmetry constraint.

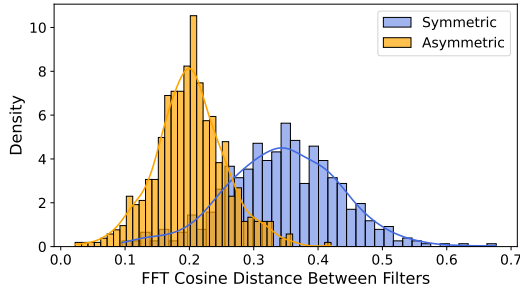


Figure 4: Distribution of pairwise cosine distances between the FFT magnitude spectra of learned filters for symmetric and asymmetric convolutions on the WISDM dataset.

**Frequency-Domain Filter Diversity** We assessed filter diversity by analysing the pairwise cosine distances between the normalised FFT magnitude spectra of the learned convolutional filters, as shown in Fig. 4. This frequency-domain analysis is particularly meaningful for time series and signal processing applications, where representing a broad range of frequency components is crucial for effective and interpretable feature extraction. The distribution of pairwise FFT cosine distances for symmetric filters (blue) is distinctly shifted towards higher values compared to asymmetric filters (orange), indicating that symmetry constraints lead to a substantially greater diversity of frequency responses and reduced spectral redundancy. Quantitatively, the mean FFT cosine distance for symmetric filters was 0.345, compared to 0.201 for asymmetric filters, with respective medians of 0.347 and 0.202. This difference is highly significant, as confirmed by the Mann-Whitney U test ( $U = 2.53 \times 10^5$ ,  $p \approx 1.1 \cdot 10^{-121}$ ). Here, symmetry constraints act as a form of regularisation, meaning they structure and constrain the space of possible filters to avoid redundancy and encourage more diverse, well-distributed frequency selectivity.

To further illustrate this diversity, we selected for each kernel size the pair of filters with the largest cosine distance between their normalised FFT magnitude spectra. Figure 5 visualises these pairs for kernel size 31. For the symmetric filters, filters 6 and 7 were identified as the most different (cosine similarity 0.323), while for the asymmetric, filters 9 and 14 formed the most dissimilar pair (cosine similarity 0.643). The symmetric filters exhibit more distinct, well-separated frequency profiles, particularly showing a clear separation between high- and low-frequency selectivity. In contrast, the asymmetric filters do not demonstrate such a distinction, instead presenting considerable overlap across the frequency spectrum.

## 7. Limitations and Future Work

While PRISM achieves good performance and remarkable efficiency by processing each sensor channel independently, this design inherently omits explicit cross-channel interactions. Although this independence contributes to the model’s lightweight structure and scalability, certain applications may benefit from selectively integrating cross-channel coupling to capture inter-modal dependencies. Exploring mechanisms for

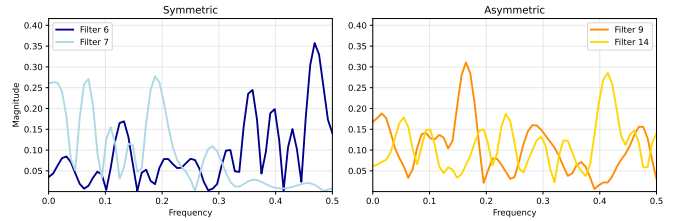


Figure 5: Frequency responses of the most dissimilar filter pairs (by cosine similarity of FFT spectrum) for kernel size 31, for both symmetric (left) and asymmetric (right) filters.

efficient cross-channel interaction, without sacrificing PRISM’s computational and parameter efficiency, represents a promising direction for future research.

Another promising avenue for improvement lies in the area of self-supervised pre-training. Recent advances in time-series modeling have shown the value of leveraging large corpora of unlabeled data through objectives such as masked-segment reconstruction or contrastive learning. Adapting such self-supervised objectives for PRISM could further improve initialisation, accuracy, and sample efficiency, particularly in data-scarce scenarios.

## 8. Conclusion

In conclusion, this paper introduced PRISM (Per-channel Resolution-Informed Symmetric Module), a novel convolution-based feature extractor designed specifically for multivariate time series classification. PRISM leverages symmetric finite impulse response (FIR) filters across multiple temporal resolutions to learn frequency-selective, phase-consistent embeddings with substantial computational efficiency and reduced parameter complexity.

Empirical evaluations across diverse benchmark datasets demonstrated PRISM’s superior or comparable predictive accuracy relative to established state-of-the-art Transformer and convolutional methods, confirming the efficacy of combining classical signal processing principles with modern convolutional architectures. Critically, PRISM achieved these results with significantly fewer parameters and reduced computational overhead, highlighting its particular suitability for resource-constrained environments and multi-dimensional applications.

Detailed ablation studies show the importance of the multi-resolution approach and the inherent benefits of symmetric filtering, revealing enhanced spectral diversity and reduced spectral redundancy. These characteristics facilitated by PRISM’s design contribute to both its performance and limited footprint, essential qualities for practical deployment.

Thus, PRISM not only addresses the prevalent issues of computational complexity and excessive parameterisation inherent in many contemporary models but also provides a robust framework adaptable across multiple time series domains and sensor modalities. This research shows the promising synergy between classical and contemporary methodologies, representing a step forwards for efficient, scalable, and expressive solutions in time series analysis.

## Acknowledgments

The work of Federico Zucchi has received funding from the Horizon Europe research and innovation programme, under grant agreement No 101095436 and Horizon European innovation council under grant agreement No. 190129251.

## References

- [1] Q. Wen, T. Zhou, C. Zhang, W. Chen, Z. Ma, Z. Yan, J. Yan, L. Sun, Transformers in time series: A survey, *International Joint Conference on Artificial Intelligence* (2023).
- [2] K. Li, Y. Wang, P. Gao, G. Song, Y. Liu, H. Li, Y. Qiao, UniFormer: Unified transformer for efficient spatiotemporal representation learning (2022).
- [3] W. Wang, E. Zuo, C. Chen, C. Chen, J. Zhong, Z. Yan, X. Lv, Efficient time series adaptive representation learning via dynamic routing sparse attention, *Pattern Recognition* (2025).
- [4] T. Zhang, Y. Zhang, W. Cao, J. Bian, X. Yi, S. Zheng, J. Li, Less is more: Fast multivariate time series forecasting with light sampling-oriented mlp structures., *arXiv preprint arXiv:2207.01186* (2022).
- [5] Y. Gu, X. Yan, H. Qin, N. Akhtar, S. Yuan, H. Fu, S. Yang, A. Mian, HDTCNet: A hybrid-dimensional convolutional network for multivariate time series classification, *Pattern Recognition* (2025).
- [6] H. Wu, T. Hu, Y. Liu, H. Zhou, J. Wang, M. Long, Timesnet: Temporal 2d-variation modeling for general time series analysis, in: *International Conference on Learning Representations*, 2023.
- [7] K. Yi, J. Fei, Q. Zhang, H. He, S. Hao, D. Lian, W. Fan, FilterNet: Harnessing frequency filters for time series forecasting, in: *Neural Information Processing Systems*, 2024.
- [8] S. G. Mallat, A theory for multiresolution signal decomposition: the wavelet representation, *IEEE transactions on pattern analysis and machine intelligence* (1989).
- [9] G. Chen, T. D. Bui, A. Krzyżak, Invariant pattern recognition using radon, dual-tree complex wavelet and fourier transforms, *Pattern Recognition* (2009).
- [10] A. V. Oppenheim, R. W. Schaffer, J. R. Buck, *Discrete-Time Signal Processing*, 3rd Edition, Prentice-Hall, 2010, section 7.4: “Linear-Phase FIR Filters”.
- [11] G. Dzhelyan, H. Cecotti, Symmetrical filters in convolutional neural networks, *International Journal of Machine Learning and Cybernetics* (2021).
- [12] S. A. Martucci, Symmetric convolution and the discrete sine and cosine transforms, *IEEE Transactions on Signal Processing* (1994).
- [13] N. Ahmed, T. Natarajan, K. R. Rao, Discrete cosine transform, *IEEE transactions on Computers* (2006).
- [14] M. Ulicny, V. A. Krylov, R. Dahyot, Harmonic convolutional networks based on discrete cosine transform, *Pattern Recognition* (2022).
- [15] K. Xu, M. Qin, F. Sun, Y. Wang, Y.-K. Chen, F. Ren, Learning in the frequency domain, in: *Proceedings of the IEEE/CVF conference on computer vision and pattern recognition*, 2020.
- [16] A. Vaswani, N. Shazeer, N. Parmar, J. Uszkoreit, L. Jones, A. N. Gomez, Łukasz Kaiser, I. Polosukhin, Attention is all you need, in: *Advances in Neural Information Processing Systems*, 2017.
- [17] H. Wu, J. Xu, J. Wang, M. Long, Autoformer: Decomposition transformers with auto-correlation for long-term series forecasting, in: *Advances in Neural Information Processing Systems*, 2021.
- [18] T. Zhou, Q. Zhang, W. Chen, H. Wu, Z. Xie, Z. Yan, Y. Wang, L. Sun, FEDformer: Frequency enhanced decomposed transformer for long-term series forecasting, in: *International Conference on Learning Representations*, 2022.
- [19] Y. Li, Z. Zhang, M. Zaheer, S. Kottur, Enhancing the locality and breaking the memory bottleneck of transformer on time series forecasting, in: *Advances in Neural Information Processing Systems*, 2020.
- [20] N. Kitaev, Ł. Kaiser, A. Levskaya, Reformer: The efficient transformer, in: *International Conference on Learning Representations*, 2020.
- [21] C. Zhang, Z. Yan, Crossformer: Transformer utilizing cross-dimension dependency for multivariate time series forecasting, in: *International Conference on Learning Representations*, 2023.
- [22] A. Zeng, M. Zhang, G. Gao, Z. Meng, J. Wang, J. Zhou, Are transformers all you need for long-term series forecasting?, in: *Neural Information Processing Systems*, 2023.
- [23] Y. Liu, Y. Zhang, H. Wu, M. Long, J. Wang, DLinear: Are linear time-series models really that simple?, in: *AAAI 2023*, 2023.
- [24] Y. Xin, Z. Ma, T. Wei, Y. Liu, Efficient attention mechanisms for long-sequence time-series modeling, in: *ACM SIGKDD*, 2024.
- [25] A. Dempster, F. Petitjean, G. I. Webb, ROCKET: Exceptionally fast and accurate time series classification using random convolutional kernels, *Data Mining and Knowledge Discovery* (2020).
- [26] E. Eldele, S. Qu, X. Wu, Z. Cao, J. Ng, TS-TCC: Time-series representation learning via temporal and contextual contrasting, in: *International Joint Conference on Artificial Intelligence*, 2021.
- [27] Z. Yue, G. Zhou, Q. Yang, S. Xu, Q. Kan, TS2Vec: Towards universal representation of time series, in: *AAAI Conference on Artificial Intelligence*, 2022.
- [28] Q. Meng, H. Qian, Y. Liu, L. Cui, Y. Xu, Z. Shen, MHCCL: masked hierarchical cluster-wise contrastive learning for multivariate time series, in: *AAAI Conference on Artificial Intelligence*, 2023.
- [29] P. Liu, Q. Kong, L. Jian, J. Kuang, T-WaveNet: A tree-structured wavelet neural network for time-series signal analysis, in: *International Conference on Learning Representations*, 2022.
- [30] P. Liu, M. Zhang, C. Li, Q. Li, N. Laptev, SCINet: Time series modeling and forecasting with sample-convolve-interact networks, in: *International Conference on Learning Representations*, 2022.
- [31] P. Liu, B. Wu, N. Li, T. Dai, F. Lei, J. Bao, Y. Jiang, S.-T. Xia, WFTNet: Exploiting global and local periodicity in long-term time series forecasting, in: *ACM SIGKDD*, 2023.
- [32] F. Zhang, C. Zhang, W. Chen, Z. Ma, TCE: Temporal convolutional explorer helps understand 1d-cnns from the frequency perspective, in: *ACM CIKM 2023*, 2023.
- [33] Y. Yang, H.-S. Hong, BTSF: Bilinear temporal-spectral fusion for unsupervised time-series representation learning, in: *International Conference on Learning Representations*, 2022.
- [34] A. L. Goldberger, L. A. Amaral, L. Glass, J. M. Hausdorff, P. C. Ivanov, R. G. Mark, J. E. Mietus, G. B. Moody, C.-K. Peng, H. E. Stanley, PhysioBank, PhysiToolKit, and PhysioNet: components of a new research resource for complex physiologic signals, *circulation* (2000).
- [35] E. Eldele, Z. Chen, C. Liu, M. Wu, C.-K. Kwok, X. Li, C. Guan, An attention-based deep learning approach for sleep stage classification with single-channel EEG, *IEEE Transactions on Neural Systems and Rehabilitation Engineering* (2021).
- [36] E. Eldele, M. Ragab, Z. Chen, M. Wu, X. Li, TSLANet: Rethinking transformers for time series representation learning, in: *International Conference on Machine Learning*, 2024.
- [37] G. B. Moody, R. G. Mark, The impact of the mit-bih arrhythmia database, *IEEE engineering in medicine and biology magazine* (2001).
- [38] A. Goldberger, UEA archive: Heartbeat data set (2016).
- [39] D. Anguita, A. Ghio, L. Oneto, X. Parra, J. L. Reyes-Ortiz, et al., A public domain dataset for human activity recognition using smartphones., in: *Esann*, 2013.
- [40] J. R. Kwapisz, G. M. Weiss, S. A. Moore, Activity recognition using cell phone accelerometers, *ACM SigKDD Explorations Newsletter* (2011).
- [41] A. Stisen, H. Blunck, S. Bhattacharya, T. S. Prentow, M. B. Kjærgaard, A. Dey, T. Sonne, M. M. Jensen, Smart devices are different: Assessing and mitigating mobile sensing heterogeneities for activity recognition, in: *Proceedings of the ACM conference on embedded networked sensor systems*, 2015.
- [42] T. Zhou, P. Niu, L. Sun, R. Jin, et al., One fits all: Power general time series analysis by pretrained LM, *Advances in neural information processing systems* (2023).
- [43] Y. Nie, N. H. Nguyen, P. Sinthong, J. Kalagnanam, A time series is worth 64 words: Long-term forecasting with transformers, in: *International Conference on Learning Representations*, 2023.
- [44] S. Khalighi, T. Sousa, J. M. Santos, U. Nunes, ISRUC-Sleep: A comprehensive public dataset for sleep researchers, *Computer methods and programs in biomedicine* (2016).
- [45] S. Goerttler, Y. Wang, E. Eldele, M. Wu, F. He, MSA-CNN: A lightweight multi-scale CNN with attention for sleep stage classification, *arXiv preprint arXiv:2501.02949* (2025).
- [46] A. Supratak, H. Dong, C. Wu, Y. Guo, DeepSleepNet: A model for auto-

- matic sleep stage scoring based on raw single-channel eeg, *IEEE transactions on neural systems and rehabilitation engineering* (2017).
- [47] V. J. Lawhern, A. J. Solon, N. R. Waytowich, S. M. Gordon, C. P. Hung, B. J. Lance, EEGNet: a compact convolutional neural network for eeg-based brain–computer interfaces, *Journal of neural engineering* (2018).
  - [48] Z. Jia, Y. Lin, J. Wang, X. Ning, Y. He, R. Zhou, Y. Zhou, L.-w. H. Lehman, Multi-view spatial-temporal graph convolutional networks with domain generalization for sleep stage classification, *IEEE Transactions on Neural Systems and Rehabilitation Engineering* (2021).
  - [49] X. Ji, Y. Li, P. Wen, Jumping knowledge based spatial-temporal graph convolutional networks for automatic sleep stage classification, *IEEE Transactions on Neural Systems and Rehabilitation Engineering* (2022).
  - [50] Y. Wang, M. Wu, X. Li, L. Xie, Z. Chen, Multivariate time-series representation learning via hierarchical correlation pooling boosted graph neural network, *IEEE Transactions on Artificial Intelligence* (2023).
  - [51] Y. Wang, Y. Xu, J. Yang, M. Wu, X. Li, L. Xie, Z. Chen, Fully-connected spatial-temporal graph for multivariate time-series data, in: *AAAI conference on artificial intelligence*, 2024.
  - [52] Z. Yang, M. Qiu, X. Fan, G. Dai, W. Ma, X. Peng, X. Fu, Y. Li, cVAN: A novel sleep staging method via cross-view alignment network, *IEEE Journal of Biomedical and Health Informatics* (2024).